Numerical Heat Transfer, Part A, 52: 991–1007, 2007

ISSN: 1040-7782 print/1521-0634 online
DOI: 10.1080/10407780701364379

Taylor & Francis
Taylor & Francis Group

NUMERICAL STUDY OF FILM AND REGENERATIVE COOLING IN A THRUST CHAMBER AT HIGH PRESSURE

H. W. Zhang, Y. L. He, and W. Q. Tao
State Key Laboratory of Multiphase Flow in Power Engineering, Xi'an Jiaotong University, Xi'an, People's Republic of China

Numerical study of coupled heat transfer of gas flow with film cooling, chamber wall conduction, and regeneration coolant cooling in the thrust chamber of a liquid rocket engine was performed. A one-dimensional model was adopted for regeneration cooling to couple two-dimensional model simulation in the thrust camber. Numerical results show that the method adopted can simulate the gas flow field well, and can calculate the heat flux through the wall, the wall temperature, and the temperature increase of the coolant quickly. In addition, liquid film cooling can reduce the wall temperature greatly, and decrease the heat flux transferred from the hot gas to the chamber wall.

INTRODUCTION

The development of liquid rocket engines, especially the trend toward higher combustion chamber pressures, leads to a large increase in the heat flux from the working fluid to the walls of the combustion chamber and the exhaust nozzle. In addition, it is expected that the engine should be used repeatedly, so as to reduce the cost. All these motivations require that effective cooling techniques be adopted to protect the surface of the walls from thermal damage caused by a hot fluid stream.

Film cooling provides an attractive means of protecting the surface of the combustion chamber and the exhaust nozzle walls from thermal damage by a hot fluid stream. A thin continuous coolant layer is injected between the wall surface and the hot fluid stream and forms a low-temperature film, decreasing the normally expected convective heat flux and providing thermal protection for the walls. The coolant may be gas or liquid, depending on the practical situation. In this article, only liquid film cooling is concerned.

Studies on liquid film cooling at low pressure have been carried out in a number of investigations. These include theoretical and experimental studies [1, 2] and numerical investigations [3, 4]. It has been shown that the latent heat is significant

Received 27 August 2006; accepted 27 February 2007.

The work reported here is supported by the National Natural Science Foundation of China (50476046), the National Science Fund for Distinguished Young Scholars from the National Natural Science Foundation of China (50425620), and the National Key Fundamental Project of R & D of China (2007BC600902).

Address correspondence to Wen-Quań Tao, State Key Laboratory of Multiphase Flow in Power Engineering, School of Energy and Power Engineering, Xi'an Jiaotong University, 28 Xi'an Ning Road, Xi'an, Shaanxi 7100 49, People's Republic of China. E-mail: wqtao@mail.xjtu.edu.cn

NOMENCLATURE

A	section area of the generation cooling tunnel, m^2	q_r^+	radial radiation heat flux point to wall, W/m^2
A_b	area at the base of the regeneration cooling tunnel, m^2	q_r^-	radial radiation heat flux point to center, W/m^2
A_f	area of fins in contact with regeneration coolant, m^2	q_w	heat flux from gas to wall, W/m^2
A_{wc}	area of heat transfer between the coolant and the surrounding wall, m^2	r	coordinate in r direction, m
A_{wh}	area of wall contact with gas, m^2	R	universal gas constant, J/mol K
c	mass fraction of film coolant	s	distance in regeneration coolant flow direction, m
c_p	constant-pressure specific heat, J/kg K	T	temperature, K
c_{pa}	constant-pressure specific heat of pure gas, J/kg K	T_r	reduced temperature
c_{pv}	constant-pressure specific heat of film coolant, J/kg K	T_{wc}	temperature of internal wall next to the regeneration coolant, K
D	mass diffusivity, m^2/s; hydrodynamic diameter of cooling channel, m	T_{wh}	temperature of wall next to the gas, K
f	Darcy friction factor	u	axial velocity, m/s
G	mass flux of nitrogen, kg/s	u_c	velocity of regeneration coolant, m/s
h	enthalpy, J/kg; external combined heat transfer coefficient, W/m^2 K	**U**	vector of velocity, m/s
h_c	convective heat transfer coefficient between the regeneration coolant and the wall, W/m^2 K	v	radial velocity, m/s
k	turbulent kinetic energy, m^2/s^2; thermal conductivity of wall, W/m K	x	axial coordinate, m
MB	ratio of mass flux of liquid film coolant to gas flow	ε	rate of dissipation of turbulent energy, m^2/s^3
p	pressure, Pa	η	dynamic viscosity, kg/m s; fin efficiency
p_r	reduced pressure	λ	thermal conductivity, W/m K
q_c	heat flux at regeneration cooling side, W/m^2	ρ	density, kg/m^3
		Subscripts	
		c	regeneration coolant
		t	turbulent
		w	wall
		0	condition at inlet

for liquid film cooling at low pressure [4]. However, studies on liquid film cooling at high pressure [5, 6] have found that the cooling mechanism of liquid film at high pressure is different from that at low pressure. At high pressure, the effect of latent heat becomes weakened because the latent heat of vaporization decreases with pressure increase; furthermore, liquid film may transit to the supercritical emission regime before dryout, and the higher the pressure, the sooner the liquid film transition to the supercritical emission regime in which the interface vanishes and the latent heat of vaporization reduces to zero. In the supercritical regime, the flow is similar to single-phase flow, and all of the thermal energy transferred from the hot gases is devoted to heating up the film [5, 6]. However, it is difficult to determine the exact location where the liquid film transits from subcritical to supercritical evaporation regime for a liquid O_2/kerosene rocket engine at high pressure. Fortunately, it has been found [5, 6] that at a very high pressure and temperature, such as $p_r > 6.0$ and $T_r > 5.0$, the liquid film transit to supercritical regime occurs at the moment it is ejected into the chamber. Because of this fact, the fluid flow in the cooling liquid film and in the gases can be simplified greatly and treated as a single-phase fluid flow.

In addition to liquid film cooling, regenerative cooling is a usual technique adopted for liquid rocket engines with huge thrust. The adoption of both liquid film cooling and regenerative cooling makes the heat transfer between the high-temperature gases in the thrust chamber and the coolant outside the chamber inner wall strongly coupled. The main focus of the present study is to investigate numerically the fluid flow and heat transfer characteristics in a thrust chamber with both liquid film cooling and regenerative cooling techniques. In the following, some related publications are reviewed briefly.

Investigation of regenerative cooling has been performed numerically in some studies, such as those of Carlos et al. [7], Niu et al. [8], Han [9], Li and Liu [10], and Toyama [11]). In these reports, the gas flow and heat transfer in the chamber were either computed by one-dimensional models or were not considered at all. Li and Liu [12] simulated the heat transfer in a regeneratively cooled nozzle, in which the coupled heat transfer between the gases in the thrust chamber and the coolant was considered and three-dimensional governing equations were solved in a coupled manner. Such computation is complicated and very time-consuming.

One-dimensional correlation is inadequate for calculating heat transfer in a rocket engine nozzle, because it cannot take some important effects (such as those of varying components of gases on heat transfer) into account. Especially, when other internal cooling techniques such as film cooling are applied as a supplement, this method cannot even qualitatively compute the heat transfer correctly.

In the present study, attention is concentrated on the flow and heat transfer characteristics of film and regenerative cooling in a thrust chamber at high pressure. The thrust chamber consists of two parts: the combustion chamber and the nozzle. The coupled heat transfer between the hot gases, cooling film, and the regenerative cooling coolant in the cooling tunnel is our major concern. The gases and film flow at high pressure in the chamber are regarded as a single-phase flow and described by two-dimensional Navier-Stokes equations and energy equation, while the coolant flow and heat transfer in the cooling tunnel is computed using a one-dimensional model.

In the following, the physical and mathematical models are first presented, followed by the turbulence model and fluid state equation. Then the determination of the fluid thermophysical properties and numerical approach is described. In the presentation of the numerical results, an analysis of the effects of film cooling on the flow and heat transfer near the wall is first provided, followed by a discussion of cooling efficiency with or without film cooling at different regeneration coolant mass fluxes, and the mutual effect of the multicooling annulus. Finally, some conclusions are drawn.

MATHEMATICAL FORMULATION

The gas flow in the thrust chamber is assumed to be in steady state, axis-symmetrical, and two-dimensioanl. Because of the high pressure and high temperature in the combustion chamber, the film coolant is supposed to reach the supercritical state at the moment it is ejected into the thrust chamber, according to previous study [6], and thus the model can be simplified greatly. To simplify the computation, a one-dimensional model is adopted to simulate the flow and heat transfer of the regenerative cooling. Other main assumptions are as follows. (1) The combustion

process is completed instantaneously and sufficiently, and the free-stream gas consists of the combustion products of fuel/oxygen. (2) The viscous dissipation effect is negligible. (3) The axial diffusion and radiation of the gas are neglected in comparison with the convection heat transfer.

Gas Governing Equations

The time-averaged Navier-Stokes equations for steady two-dimensional compressible gas flow in cylindrical coordinates can be written as follows.
Continuity equation:

$$\frac{1}{r}\frac{\partial(r\rho v)}{\partial r}+\frac{\partial(\rho u)}{\partial u}=0 \tag{1}$$

Axial momentum equation:

$$\frac{\partial}{\partial x}(\rho uu)+\frac{1}{r}\frac{\partial}{\partial r}(r\rho vu)=\frac{\partial}{\partial x}\left(\eta_{\text{eff}}\frac{\partial u}{\partial x}\right)+\frac{1}{r}\frac{\partial}{\partial r}\left(\eta_{\text{eff}}r\frac{\partial u}{\partial r}\right)+S_u \tag{2}$$

Radial momentum equation:

$$\frac{\partial}{\partial x}(\rho uv)+\frac{1}{r}\frac{\partial}{\partial r}(r\rho vv)=\frac{\partial}{\partial x}\left(\eta_{\text{eff}}\frac{\partial v}{\partial x}\right)+\frac{1}{r}\frac{\partial}{\partial r}\left(\eta_{\text{eff}}r\frac{\partial v}{\partial r}\right)+S_v \tag{3}$$

Energy equation:

$$\frac{\partial}{\partial x}(\rho uh)+\frac{1}{r}\frac{\partial}{\partial r}(r\rho vh)=\frac{\partial}{\partial x}\left[(\lambda+\lambda_t)\frac{\partial T}{\partial x}\right]+\frac{1}{r}\frac{\partial}{\partial r}\left[r(\lambda+\lambda_t)\frac{\partial T}{\partial r}\right]+S_T \tag{4}$$

Concentration equation for film:

$$\frac{\partial(\rho uc)}{\partial x}+\frac{1}{r}\frac{\partial(r\rho vc)}{\partial r}=\frac{\partial[\rho(D+D_t)\partial c/\partial r]}{\partial x}+\frac{1}{r}\frac{\partial[r\rho(D+D_t)\partial c/\partial r]}{\partial r} \tag{5}$$

where

$$\eta_{\text{eff}}=\eta+\eta_t \tag{6}$$

$$S_u=-\frac{\partial p}{\partial x}+\frac{\partial}{\partial x}\left(\eta_{\text{eff}}\frac{\partial u}{\partial x}\right)+\frac{1}{r}\frac{\partial}{\partial r}\left(r\eta_{\text{eff}}\frac{\partial v}{\partial x}\right)+\frac{\partial}{\partial x}\left(-\frac{2}{3}\eta_{\text{eff}}\,\text{div}\,\mathbf{U}\right) \tag{7}$$

$$\begin{aligned}S_v=&-\frac{\partial p}{\partial r}+\frac{\partial}{\partial x}\left(\eta_{\text{eff}}\frac{\partial u}{\partial r}\right)+\frac{1}{r}\frac{\partial}{\partial r}\left(r\eta_{\text{eff}}\frac{\partial v}{\partial r}\right)\\&-\frac{2\eta_{\text{eff}}v}{r^2}+\frac{\rho w^2}{r}+\frac{1}{r}\frac{\partial}{\partial r}\left(-\frac{2}{3}r\eta_{\text{eff}}\,\text{div}\,\mathbf{U}\right)+\frac{2}{3}\frac{\eta_{\text{eff}}}{r}\,\text{div}\,\mathbf{U}\end{aligned} \tag{8}$$

$$S_T = [\mathrm{div}(p\mathbf{U}) - p\,\mathrm{div}\,\mathbf{U}] + \Phi + \rho_G(D + D_t)\frac{c_{pv} - c_{pa}}{c_{pG}}\frac{\partial T}{\partial r}\frac{\partial c}{\partial r} + S_r \tag{9}$$

$$\mathrm{div}\,\mathbf{U} = \frac{1}{r}\frac{\partial(rv)}{\partial r} + \frac{\partial u}{\partial x} \tag{10}$$

$$\Phi = \eta_t\left\{2\left[\left(\frac{\partial u}{\partial x}\right)^2 + \left(\frac{\partial v}{\partial r}\right)^2 + \left(\frac{v}{r}\right)^2\right] + \left(\frac{\partial u}{\partial r} + \frac{\partial v}{\partial x}\right)^2\right\} \tag{11}$$

where S_r is the source term resulting from the gas radiation, and its expression is given later.

Gases are presumed to be the production of the fuel and oxidant, and the properties are obtained from thermodynamic computation. Presuming that the gases are in chemical equilibrium state, their thermophysic properties are functions of temperature and pressure. In the present article, gases are dealt with as real gases, so their state equation can be written as

$$pv = ZRT \tag{12}$$

Radiation Model

To calculate the radiant heat flux of gases, the FLUX model is adopted [13]. For simplicity, the radiation in the axial direction is neglected. Then the radiant heat flux of radial direction can be expressed as

$$\frac{dq_r^+}{dr} = -(a + \sigma_s)q_r^+ + aE_b + \frac{\sigma_s}{2}(q_r^+ + q_r^-) - \frac{q_r^+ - q_r^-}{r} \tag{13}$$

$$\frac{dq_r^-}{dr} = (a + \sigma_s)q_r^- - aE_b - \frac{\sigma_s}{2}(q_r^+ + q_r^-) \tag{14}$$

where $E_b = \sigma T^4$ and q_r^+ and q_r^- are the radiant heat fluxes pointing to the wall and the center, respectively.

The boundary condition for the radiant heat flux is

$$r = 0 \qquad q_r^+ = q_r^- \tag{15}$$

$$r = R \qquad q_{r,w}^- = \varepsilon_w E_{bw} + (1 - \varepsilon_w)q_{r,w}^+ \tag{16}$$

The gas radiant heat flux source term in the energy equation can be expressed by

$$S_r \equiv \Phi_r == -\frac{1}{r}\frac{d(rq_r^+ - rq_r^-)}{dr} \tag{17}$$

Turbulence Model

The low-Reynolds-number k–ε model [14] is adopted to define the thin film and gas turbulence flow. The transport equations for k and ε are

$$\frac{\partial}{\partial x}\left(\rho u\frac{\partial k}{\partial x}\right)+\frac{1}{r}\frac{\partial}{\partial r}\left(r\rho v\frac{\partial k}{\partial r}\right)=\frac{\partial}{\partial x}\left[\left(\eta+\frac{\eta_t}{\sigma_k}\right)\frac{\partial k}{\partial x}\right]+\frac{1}{r}\frac{\partial}{\partial r}\left[r\left(\eta+\frac{\eta_t}{\sigma_k}\right)\frac{\partial k}{\partial r}\right]+G-\rho\varepsilon-D \tag{18}$$

$$\frac{\partial}{\partial x}\left(\rho u\frac{\partial \varepsilon}{\partial x}\right)+\frac{1}{r}\frac{\partial}{\partial r}\left(r\rho v\frac{\partial \varepsilon}{\partial r}\right)=\frac{\partial}{\partial x}\left[\left(\eta+\frac{\eta_t}{\sigma_\varepsilon}\right)\frac{\partial \varepsilon}{\partial x}\right]+\frac{1}{r}\frac{\partial}{\partial r}\left[r\left(\eta+\frac{\eta_t}{\sigma_\varepsilon}\right)\frac{\partial \varepsilon}{\partial r}\right]+C_1|f_1|\frac{\varepsilon}{k}G-C_2|f_2|\rho\frac{\varepsilon^2}{k}+E \tag{19}$$

where the turbulence viscosity is expressed as

$$\eta_t=\rho f_\mu C_\mu k^2/\varepsilon \tag{20}$$

In Eqs. (18) and (19), G is the generation term and can be calculated by

$$G=\eta_t\left\{2\left[\left(\frac{\partial u}{\partial x}\right)^2+\left(\frac{\partial v}{\partial r}\right)^2+\left(\frac{v}{r}\right)^2\right]+\left(\frac{\partial u}{\partial r}+\frac{\partial v}{\partial x}\right)^2\right\} \tag{21}$$

Other parameters in Eqs. (18) and (19) are listed in Table 1.

Regeneration Coolant Flow Governing Equations

In this study the coolant is injected with a specific mass rate into the cooling tunnel (Figure 1). The configuration of the cooling tunnel is shown in Figure 2.

The main simplification used in the regenerative cooling simulation with respect to the real problem is to regard the coolant flow as one-dimensional. Since the individual channel dimension is relatively small (see Figure 2), this assumption is quite acceptable, at least from an engineering point of view. The mass conservation equation, the momentum equation, and the energy equation of the coolant are expressed respectively as follows [7]:

$$\frac{d}{ds}(\rho_c u_c A)=0 \tag{22}$$

$$\frac{d}{ds}(\rho_c u_c^2 A)=-A\frac{dp_c}{ds}+F' \tag{23}$$

$$c_{pc}\frac{d}{ds}(\rho_c u_c A T_c)=\beta T_c u_c A\frac{dp_c}{ds}+q' \tag{24}$$

Table 1. Parameters in turbulence model

c_μ	c_1	c_2	σ_k	σ_ε	f_μ	f_1	f_2	D	E
0.09	1.4	1.8	1.4	1.3	$(1+3.45\ \mathrm{Re}_t^{-1/2})\times(1-e^{-y+/70})$	1.0	$\left(1-\frac{2}{9}e^{-(\mathrm{Re}_t/6)^2}\right)\times(1-e^{-y+/5})^2$	0.	0.

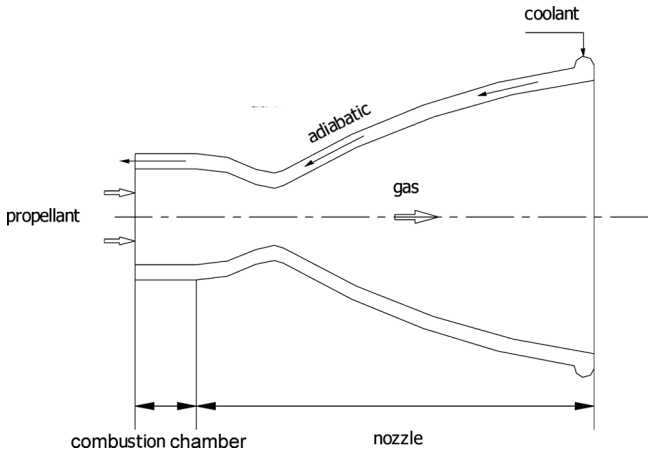

Figure 1. Schematic diagram of the regenerative cooling thrust chamber.

where F' is the tunnel drag friction and q' contains two parts: friction work and heat transfer through the wall. F' and q' are given by

$$F' = -\frac{\pi}{8} f \rho_c u_c |u_c| D \tag{25}$$

$$q' = |u_c F'| + A'_{wc} q_c \tag{26}$$

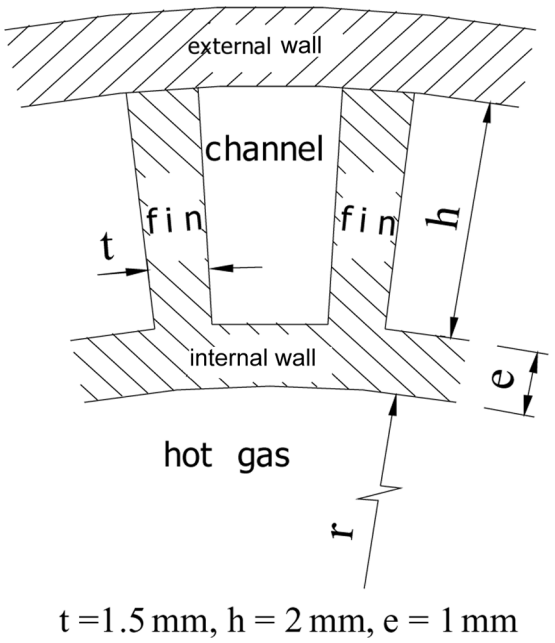

Figure 2. Configuration of regeneration cooling tunnel.

where f and D represent the Darcy friction factor and the hydrodynamic diameter of the cooling channel, respectively, A'_{wc} represents A_{wc} by the unit of length s, and A_{wc} is the area of heat transfer between the coolant and the surrounding wall. The heat flux q_c is given by

$$q_c = h_c(T_{wc} - T_c) \tag{27}$$

and the heat transfer surface of the surrounding wall is

$$A_{wc} = A_b + A_f \eta \tag{28}$$

In Eqs. (27) and (28) h_c represents the convective heat transfer coefficient between the coolant and the wall, T_{wc} represents the temperature of the internal wall next to the coolant, A_b is the area at the base of the channel (Figure 2) that is in contact with the coolant, A_f is the area of the fins in contact with coolant, and η represents fin efficiency [15].

To solve the governing equations, Eqs. (22)–(24), it is necessary to decide the values of the friction factor f and the convective heat transfer coefficient h_c. In the present article they are calculated by the Colebrook equation [16] and the Sieder-Tate equation for turbulent heat transfer [15], respectively. When the coolant is under the supercritical state, the convective heat transfer coefficient h_c is calculated according to [17].

Coupling of the Gas and Coolant Flows Through Heat Conduction Through the Wall

The one-dimensional steady heat transfer transfers through the wall can be written as

$$A_{wh} q_w = A_{wh} k \frac{(T_{wh} - T_{wc})}{e} = A_{wc} h_c (T_{wc} - T_c) \tag{29}$$

$$q_w = \frac{k}{e}(T_{wh} - T_{wc}) = \frac{A_{wc}}{A_{wh}} h_c (T_{wc} - T_c) = h(T_{wh} - T_c) \tag{30}$$

where q_w is the heat flux from the gas to the wall and contains two parts, convective heat flux and radiation heat flux; T_{wh} is the temperature of the wall next to the gas and T_{wc} is the temperature of the wall next to the coolant; A_{wh} is the area of the wall contact with the gas; and h represents the external combined heat transfer coefficient,

$$h = \frac{1}{e/k + A_{wh}/A_{wc} h_c} \tag{31}$$

Now the thermal boundary condition of the gas flow in the nozzle can be expressed by the third boundary condition:

$$q_w = h(T_{wh} - T_c) \tag{32}$$

NUMERICAL SOLUTION METHOD

The gas and film flow governing equations (1)–(5) and turbulence model equations (18)–(19) are discretized by the finite-volume method in body-fitted coordinates

[18] and the coupling of pressure and velocity is implemented by the compressible form of the SIMPLE algorithm [19, 20]. The convective term is approximated by the central difference scheme blended with the upwind difference scheme [20]. Each of the discretized equations forms a tridiagonal matrix equation, which can be solved by the alternating direction implicit (ADI) method. Radiation equations (13) and (14) are solved by the fourth-order Runge-Kutta method.

The total temperature, total pressure, and flow direction are prescribed for a subsonic inlet boundary. Supersonic outflow is applied to the exit, and all variables are extrapolated from internal grid values. No-slip condition is specified at the walls.

A nonuniform body-fitted grid (400×162) was generated by solving an elliptic differential equation, and its schematic distribution is shown in Figure 3. To enhance the stability of the computation, the results obtained on coarse grids with simpler models are adopted as the initial fields.

The coolant flow governing equations (22)–(24) are discretized by the finite-difference method and the convective term is approximated by the central difference scheme. The coolant velocity and temperature are fixed at the channel inlet (at the nozzle exit); the channel exit pressure is equal to the combustion pressure. The outside wall of the channel is adiabatic.

The steps adopted to solve the coupled heat transfer of the gas, wall, and regeneration coolant are as follows.

1. The values of T_c and h are assumed at any x.
2. The gas governing equations are solved to obtain the values of T_{wh} and q_w.
3. Equation (27) is solved to obtain the values of T_{wc} and q_c.
4. The regeneration coolant governing equations are solved to obtain values of T_c and h.
5. Steps 2–4 are repeated until convergence is reached.

The convergence conditions adopted are as follows. For the gas-side flow field computation,

$$\text{SMAX/FLOWIN} < 10^{-6} \tag{33a}$$

For the coolant-side iteration,

$$\max\left(\frac{T_{c,i} - T_{c,i}^0}{T_{c,i}^0}\right) < 10^{-6} \tag{33b}$$

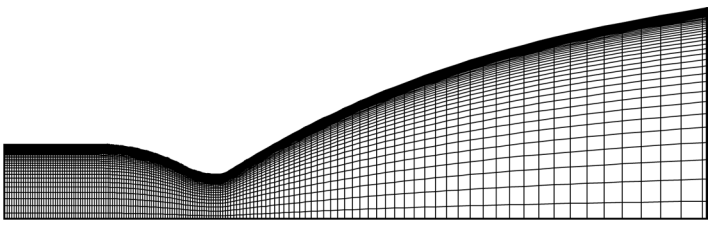

Figure 3. Rarefied grid distribution for the thrust chamber.

where SMAX is the maximum unbalance of control-volume mass flux, FLOWIN is the mass flow rate at the combustion chamber inlet, and $T^0_{c,i}$ is the value of $T_{c,i}$ at the previous iteration, in which the subscript i stands for the grid index of the coolant channel.

RESULTS AND DISCUSSION

The computation is performed for a high-pressure thrust chamber with liquid oxygen and kerosene propellants. The thrust chamber has the following characteristic parameters: The total pressure is equal to 15 MPa, and the total temperature is 3,800 K. The internal wall of the thrust chamber as well as the fins of the channel (Figure 2) are made of copper, and its thermal conductivity is 375 W/m K. The number of channels is 220. Regeneration coolant inlet temperature is prescribed as 300 K, and the pressure at the channel exit is 15 MPa. Coolant mass flux is 30 kg/s.

Three cooling annuli are placed as shown in Figure 4. The dimensionless distances $X_i[= (L_i - L_t)/L]$ of the three cooling annuli are respectively -0.25, -0.097, and -0.075. The ratios of the mass flux of film coolant to gas at each cooling annulus are 1%, 0.76%, and 0.73%, respectively.

Figure 5 shows the axial distribution of the gas convective heat flux. In view of the unavailability of experimental data, Bartz's formula [21] is adopted to compare with the present study. For comparison purposes, the first kind of thermal boundary condition is adopted for the thrust chamber wall, and its temperature is prescribed as 800 K. In Figure 5, the curve calculated by Bartz's equation is shown by the solid line, and that of our prediction by the dashed line. It can be found from Figure 5 that, except for the inlet region, the agreement between the predicted convective heat flux and that from Bartz's equation is quite good. The peak of the convective heat flux and its reduction after the peak predicted by the two methods agree with each other. The major difference between the two results is in the inlet region: Our method seems to overestimate the convective heat flux there. This is because in the present study the combustion process is not considered and the inlet total temperature is assumed to be equal to combustion chamber total temperature, which leads to the inlet gas temperature being much higher than the actual situation. There is another

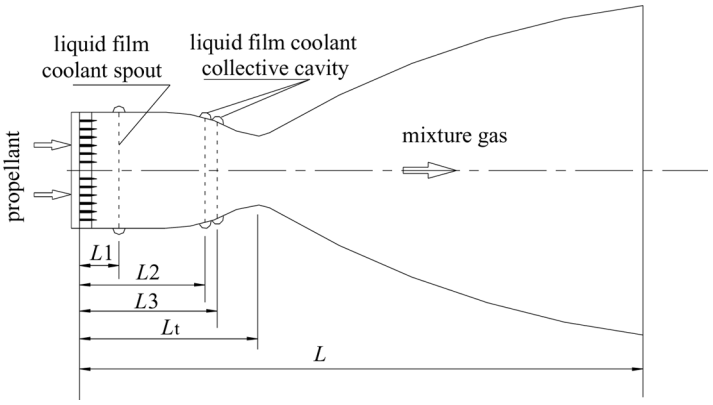

Figure 4. Schematic diagram of cooling annulus.

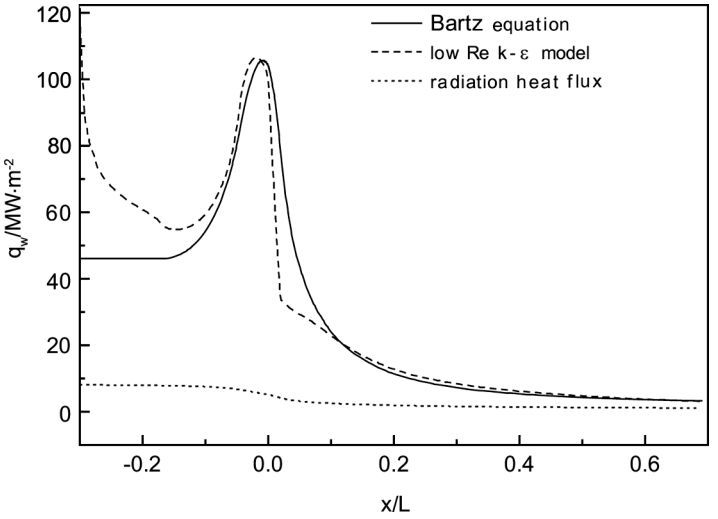

Figure 5. Distribution of heat flux along the wall with the isothermal boundary condition.

minor difference between the two results: After the flux peak, the reduction of our prediction is sharper than the Bartz prediction, but soon the reduction slows down and then it gradually comes to coincide with the curve calculated by Bartz's equation. The present authors believe that this effect is caused by the specific nozzle pattern of the present situation: There is an arc with small radius at the throat location (see Figure 4), which causes rapid gas expansion after the arc and thus a subsequent significant reduction of the gas velocity, leading to the observed variation of the convective heat flux.

Figure 5 also shows the distribution of the radiant heat flux. It is clear that the radiant heat flux is at its maximum in the combustion chamber and decreases all along the thrust chamber. The radiant heat flux decreases to about 64% of the maximum at the throat and to 12% at the exit of the nozzle. Generally speaking, the radiant heat flux is only a small part of the total heat flux. For example, it is less than 5% of the total heat flux at the throat.

For the cases with liquid film cooling, it is unfortunate that no experimental data are available to the present authors. To enhance the reliability of the computational results, the independence of the grid was tested. Numerical experiments for several grid arrangements were performed, and a comparison of the gas wall temperature for a typical case is shown in Figure 6. The deviations of the results for the two grid systems of 200×152 and 400×162 were less than 1% in most locations at the upstream of the throat. Therefore, the 400×162 grid system was chosen for subsequent computations. All the computations were performed on a personal computer with frequency of 1 M and built-in memory of 2 G.

Attention now is turned to the gas wall temperature distribution. Figure 7 shows the distribution of the gas wall temperature. When regeneration cooling alone is adopted, the gas wall temperature is very high in the combustion chamber and the convergent region of the nozzle. Just downstream of the throat, the gas wall

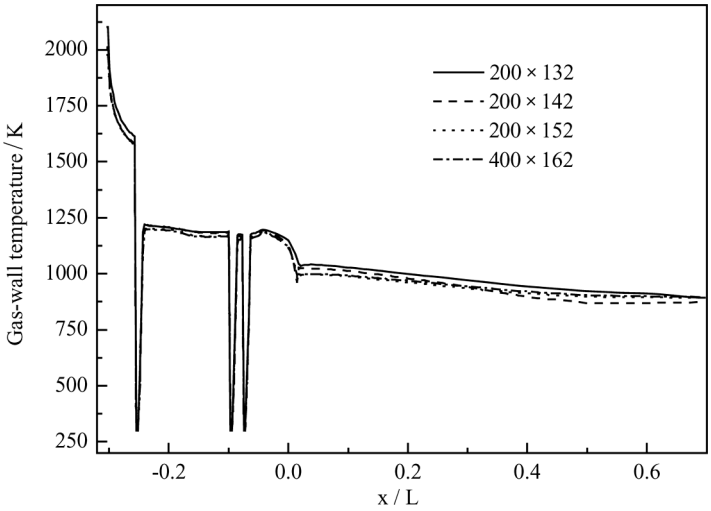

Figure 6. Axial distribution of gas wall temperature for different grids.

temperature decreases suddenly and reaches quite a low value, less than 1,000 K. After this point, the gas wall temperature rises slightly and then decreases gradually. As expected, when both film cooling and regeneration cooling are used, the gas wall temperature is much lower in the whole divergent region of the nozzle. The temperature distribution curve clearly shows that liquid film cooling can remarkably reduce the wall temperature downstream of the cooling annulus in the combustion chamber and the convergent region of the nozzle. It should be noticed that downstream of the throat, the wall temperature is higher instead of lower than that with regeneration

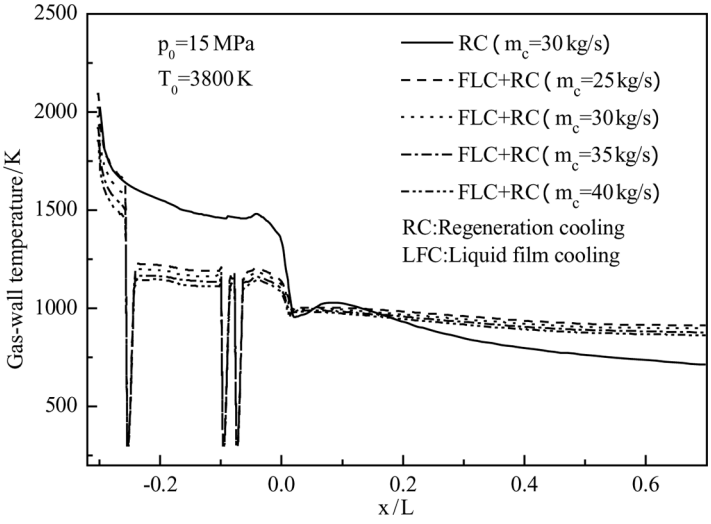

Figure 7. Axial distribution of gas wall temperature.

cooling alone. This may be caused by the difference in thermophysical properties between kerosene (the film coolant) at low pressure and the gas. The effect of the regenerative coolant mass flux on the gas wall temperature is also shown in Figure 7. It can be found that the gas wall temperature decreases with the coolant mass flux increase. This is easy to understand, because increasing the coolant mass flux enhances the regeneration cooling and hence reduces the gas wall temperature. However, the effects are not so significant downstream of the film cooling annulus as in the upstream part. It is interesting to notice that the gas wall temperature in the second case [liquid film cooling + regeneration cooling ($m_c = 25\,\mathrm{kg/s}$)] is very much lower than that in the first case [regeneration cooling only ($m_c = 30\,\mathrm{kg/s}$)]; this implies that at such condition, to apply film cooling is more effective than increasing regenerative coolant mass flux only.

The heat flux in the regenerative cooling thrust chamber is demonstrated in Figure 8. It can be found that the heat flux distribution for the case of regeneration cooling only is similar to that of isothermal condition (see Figure 5), except that the flux value is smaller. It can be clearly observed that ejection of film coolant reduces the heat flux in the combustion chamber and the throat greatly. Figure 8 also demonstrates that the heat flux increases with increase of the regenerative coolant mass flux. It should be noted that liquid film cooling can reduce both the chamber wall temperature and heat flux through the wall, while regeneration cooling alone can only reduce the wall temperature with increasing heat flux, requiring enhanced heat transfer of the regeneration cooling.

Figure 9 shows the distribution of the regeneration coolant temperature for the cases with or without liquid film cooling. The regeneration coolant temperature increases continually along the flow direction because the coolant always absorbs heat transferred from the internal wall. It is of interest to notice that for the case of regenerative cooling only, the coolant temperature increases more rapidly at the

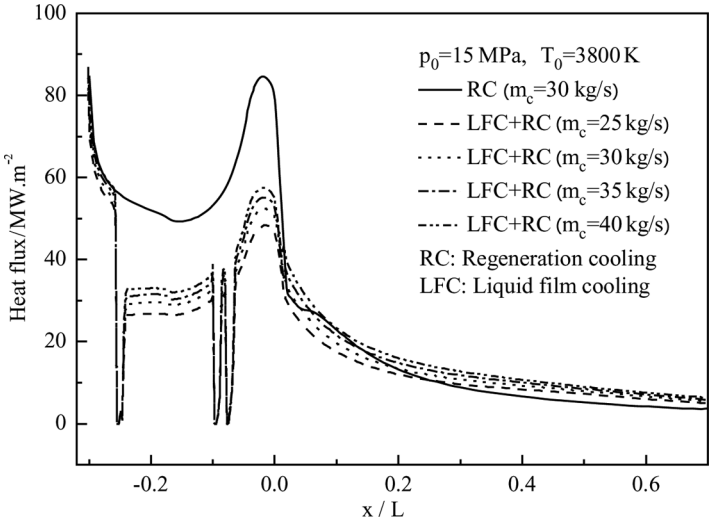

Figure 8. Axial distribution of heat flux at the chamber wall.

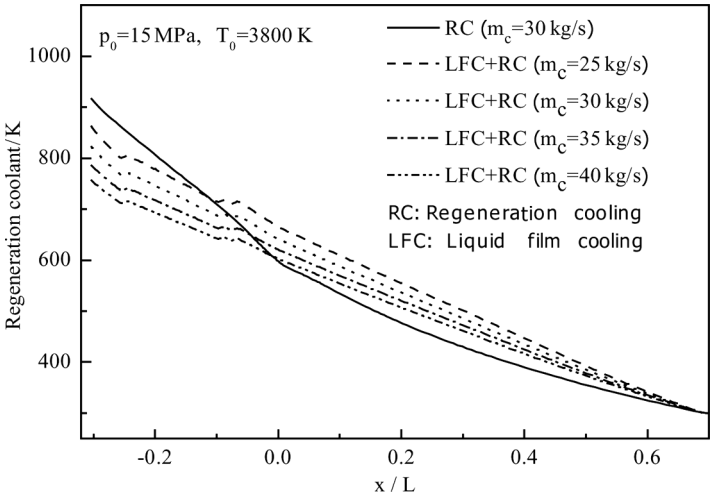

Figure 9. Distribution of regeneration coolant temperature.

upstream of the throat, because in this region the gas heat flux is large and there is more heat transfer to the coolant. For the case in which both regenerative cooling and liquid film cooling are used, the coolant temperature variation slope is more or less uniform. This is because the film cooling has decreased greatly the heat flux transferred from the gas to the regeneration coolant through the wall in the combustion chamber part, as can be seen from Figure 8. As expected, increasing regenerative coolant mass flux can decrease the regenerative coolant temperature as shown in Figure 9.

Finally, the film thickness variation along the flow direction is discussed. In the above discussion it has been pointed out when the liquid film is in the supercritical evaporation regime, the liquid–vapor interface vanishes. In this sense, the term "liquid film cooling" is not correct for flow in the supercritical regime. However, for convenience of description and for consistency with the film cooling in the subcritical regime, here we still adopt this term. Thus, in order to see the variation of film thickness in the supercritical regime, it is necessary to define the "interface" or the thickness of the film for convenience of discussion. In the literature, there are three definitions. First, the interface in the supercritical regime is defined as the location where the fluid temperature is the critical mixing temperature [22]. This definition is consistent with the definition in the subcritical regime. The second definition presumes that the fluid is the cooling film if the mass fraction of the coolant is greater than a given percentage, say 99%, and the location where the mass fraction of the coolant equals this given value is the interface [23]. Evidently, this definition belongs to the pure fluid interface. The third definition suggests that the interface is the point where the radial gradient of the coolant reaches a maximum at the section [24]. It should be noted that different definitions may lead to different thickness of the cooling film, but without any effects on flow and heat transfer of the gas and film.

Figure 10 shows the variation of the film thickness along the axial direction for the different definitions elaborated above. It can be found that the thickness of the

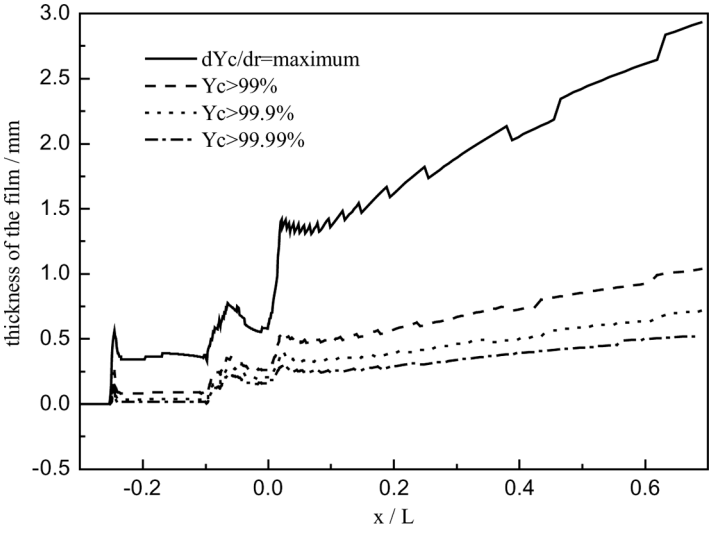

Figure 10. Variation of film thickness under different definitions.

film according to the third definition is much greater than that according to the second definition. This demonstrates that the position with the greatest gradient of coolant mass fraction is far from the pure fluid interface defined by the second definition. For the second definition, the thickness of film becomes thinner with the increase in the given percentage, which is opposite to the thickness of the flow boundary layer.

For whatever definition, the qualitative variation patterns are all the same: Generally speaking, the film thickness increases along the axial direction, and after the three injection locations, the local thickness shows an abrupt increase as a result of the ejection of coolant continuously and expansion with heat, and then decreases due to diffusion effect. At the downstream of the first cooling annulus the thickness of the film has a relatively low value. This is because the velocity of fluid in the combustion chamber is much smaller than that in the nozzle, consequently the effect of the convection is weak and diffusion plays a more important role.

As far as the film thickness at different position of the chamber is concerned, it is much greater downstream of the second and third cooling annuli, and it is also easy to find that the thickness of the film downstream of the third cooling annulus is increased, evidently due to the ejection of coolant at the second cooling annulus. The thickness of the film reaches a local minimum at the throat, and from this point on, it increases gradually because the fluid expands in the whole divergence region of the nozzle.

Finally, we ought to point out that although the coolant reaches supercritical condition at the moment of being ejected into the thrust chamber, it still forms a thin layer with low temperature, protecting the thrust chamber wall from heat damage.

CONCLUSIONS

The liquid film cooling at high pressure in a thrust chamber has been studied numerically. The coupled heat transfers between the hot gas, film cooled chamber

wall, and regeneration coolant are considered all together. Based on the numerical results obtained, the following conclusions can be drawn.

1. The method adopted in this article can solve effectively the coupled heat transfer of the hot gas, chamber wall, and regeneration coolant, and can simulate the gas two-dimensional flow field well. In addition, the heat flux through the wall, the wall temperature, and the temperature increase of the regeneration coolant can be determined effectively.
2. Liquid film cooling can reduce the wall temperature significantly, decreasing the heat flux transferred from the hot gas to the chamber wall.
3. Although the liquid film reaches supercritical emission regime at the moment of being ejected into the thrust chamber, it can form a thin layer film with low temperature and protect the wall from damage by hot gas.

REFERENCES

1. R. A. Gater, M. R. L'Ecuyer, and C. F. Warner, Liquid-Film Cooling, Its Physical Nature and Theoretical Analysis. AD Rep. TM-65-6, Jet Propulsion Center, Purdue University, West Lafayette, IN, 1965.
2. M. G. William, Liquid Film Cooling in Rocket Engines, AD Rep. AEDC-TR-91-1, Arnold Engineering Development Center, Arnold AFB, Tennessee, 1991.
3. W. M. Yan and C. Y. Soong, Numerical Study of Liquid Film Cooling in a Turbulent Gas Stream, *Int. J. Heat Mass Transfer*, vol. 36, pp. 3877–3885, 1993.
4. H. W. Zhang, W. Q. Tao, Y. L. He, and W. Zhang, Numerical Study of Liquid Film Cooling in a Rocket Combustion Chamber, *Int. J. Heat Mass Transfer*, vol. 49, pp. 349–358, 2006.
5. H. W. Zhang, Numerical Study on Liquid Film Cooling and the Characteristics of Gas Flow and Heat Transfer in Thrust Chamber at High Pressure, Ph.D. thesis, Xi'an Jiaotong University, Xi'an, China, 2006.
6. H. W. Zhang, Numerical Study on Film Cooling and the Characteristics of Gas Flow and Heat Transfer in Thrust Chamber at High Pressure, Ph.D. Thesis, Xi'an Jiaotong University, Xi'an, China, 2006.
7. H. M. Carlos, L. Fernando, F. C. da Silva Antonio, and N. H. Jose, Numerical Solutions of Flows in Rocket Engines with Regenerative Cooling, *Numer. Heat Transfer A*, vol. 45, pp. 699–717, 2004.
8. L. Niu, H. E. Cheng, and M. H. Li, Effects of Aspect Ratio and Wall Roughness on Flow in Regenerative Cooling Channels, *J. Shanghai Jiaotong Univ.*, vol. 36, pp. 1612–1615, 2002.
9. Z. X. Han, W. Lin, Y. J. Zhang, G. J. Zhu, S. L. Ji, Computing of Three-Dimensional Wall Temperature Field in Liquid Rocket Thruster Chamber, *J. Aerospace Power* (in chinese), vol. 11, pp. 145–148, 1996.
10. J. W. Li and Y. Liu, Method of Computing Temperature Field in Regeneratively-Cooled Thrust Chamber, *J. Aerospace Power*, vol. 19, pp. 550–556, 2004.
11. S. Toyama, Numerical Analysis of Nozzle Cooling for Upper-Stage Liquid Rocket Engines, 43rd AIAA Aerospace Sciences Meeting and Exhibit, Reno, NV, AIAA-2005-387, 2005.
12. J. W. Li and Y. Liu, Three Dimension Numerical Simulation of Heat Transfer in Regeneratively Cooled Nozzle, *J. Propulsion Technol.*, vol. 26, pp. 111–115, 2005.

13. E. E. Khalil, *Modelling of Furnaces and Combustors*, p. 281, Abacus Press, Kent, UK, 1982.
14. H. K. Myong and N. Kasagi, A New Approach to the Improvement of $k-\varepsilon$ Turbulence Model for Wall-Bounded Shear Flow, *Jpn. Soc. Mech. Eng. Int. J. Ser. II*, vol. 33, pp. 63–72, 1990.
15. A. Bejan, *Heat Transfer*, pp. 60, 316, Wiley, New York, 1993.
16. R. W. Miller, *Flow Measurement Engineering Handbook*, 2nd ed., p. 269, McGraw-Hill, New York, 1983.
17. D. K. Huzel and D. H. Huang, *Modern Engineering for Design of Liquid Propellant Rocket Engines*, p. 5, McGraw-Hill, New York, 1992.
18. W. Q. Tao, *Numerical Heat Transfer*, 2nd ed., pp. 442–463, Xi'an Jiaotong University Press, Xi'an, China, 2001.
19. K. C. Karki and S. V. Patankar, Pressure Based Calculation Procedure for Viscous Flows at All Speeds in Arbitrary Configurations, *AIAA J.*, vol. 27, pp. 1167–1174, 1989.
20. I. Demirdzic, Z. Lilek, and M. Peric, A Collocated Finite Volume Method for Prediction of Flows at All Speeds, *Int. J. Numer. Meth. Fluids*, vol. 16, pp. 1029–1050, 1993.
21. D. R. Bartz, A Simple Equation for Rapid Estimation of Rocket Nozzle Convective Heat Transfer Coefficients, *Jet Propulsion*, vol. 37, pp. 49–51, 1957.
22. V. Yang, N. Lin, and J. S. Shuen, Vaporization of Liquid Oxygen (LOX) Droplets in Supercritical Hydrogen Environments, *Combustion Sci. Technol.*, vol. 97, pp. 247–270, 1994.
23. K. Harstad and J. Bellan, Isolated Fluid Oxygen Drop Behavior in Fluid Hydrogen at Rocket Chamber Pressures, *Int. J. Heat Mass Transfer*, vol. 41, pp. 3537–3550, 1998.
24. K. Harstad and J. Bellan, An All-Pressure Fluid Drop Model Applied to a Binary Mixture: Heptane in Nitrogen, *Int. J. Multiphase Flow*, vol. 26, pp. 1675–1706, 2000.